

RESEARCH

Open Access



Effect of Impact Load on Splice Length of Reinforcing Bars

Hyeon-Jong Hwang¹, Fan Yang², Li Zang², Jang-Woon Baik³ and Gao Ma^{2*} 

Abstract

Impact loading damage of reinforced concrete (RC) members deteriorates bond strength of reinforcing bars. To understand the effect of strain rate on the bond strength of reinforcing bars in RC beams under impact load, drop hammer test was performed on twenty-four simply supported RC beams with lap spliced bars at the mid-span. The test parameters were reinforcing bar diameter, splice length, drop height, and hammer mass. The dynamic responses including the impact load history, mid-span deflection history, crack distribution, and strain history of reinforcing bar were evaluated. Although the designed bar development length was 31–69% of the requirement of current design codes under static load, the tensile strength of bar splices was greater than the dynamic yield strength when subjected to large impact energy under impact load. On the basis of the test results, existing design equations for the bar development length under static load were modified to consider the impact loading effect on the bond strength. Factors related to the strain rate effect of materials, impact damage, and impact energy loss were proposed. The prediction of the proposed method agreed well with the tensile strength of bar splices under impact load.

Keywords: drop hammer test, RC beam, impact load, strain rate effect, lap splice test, development length, bond strength

1 Introduction

In reinforced concrete (RC) structures, impact damage is a critical issue: piers of bridge collided by ships or other vehicles, retaining walls damaged by heavy rocks, and high-rise buildings attacked by aircraft. Particularly, impact damage on the development length of reinforcing bars may deteriorate the structural integrity significantly. However, current design codes specify the bar development length based on test results under static load. To consider the strain rate effect due to impact load on the bar development length, available studies and test results are extremely limited.

The impact resistance of RC structures depends on the material properties of concrete and reinforcing bars

under high-strain rate. Impact loads with short duration increase the material properties of concrete and reinforcing bars in different ratio, which change ductile behavior into brittle behavior in RC structures (Yang and Lok 2007). Bischoff and Perry (1991) reported the increase of 85–100% in compressive strength of concrete under impact load. According to Malvar and Ross (1998), high-strain rate increases the tensile strength of concrete more than the compressive strength of concrete. Soroushian and Choi (1987) reported that dynamic load increased both the yield and ultimate strength of reinforcing bars.

The load transfer from reinforcing bars to adjacent concrete becomes essential for the structural integrity and ductile response. Thus, understanding the bond between concrete and reinforcement in RC structures under impact load is of great importance. The existing studies reported that the bond strength increases as strain rates increase (Shah and Hansen 1963, Rezan-soff et al. 1975). Hansen and Liepins (1962) performed pull-out tests of reinforcing bars under impact load, and

*Correspondence: magao@hnu.edu.cn

² Key Laboratory for Damage Diagnosis of Engineering Structures of Hunan Province, College of Civil Engineering, Hunan University, Changsha 410082, China

Full list of author information is available at the end of the article
Journal information: ISSN 1976-0485 / eISSN 2234-1315

initially found the increase of bond strength under high-strain rate. Paschen et al. (1974) confirmed that the increase of bond strength can be attributed to the increase of concrete strength because the main mechanism of the bond is based on the concrete surrounding the ribs of the steel (or reinforcement). However, the strain rate dependency of concrete in tension and compression are observed to be different. Solomos and Berra (2010) performed dynamic Hopkinson bar tests, and the test results showed that the peak pullout force and bond stress-slip curve under high strain rates were above those of static load. Toikka et al. (2015) performed shock tube testing to investigate the strain rate effect on the bar development length under three simulated blast loads: static, 0.1 s^{-1} , and 0.2 s^{-1} . The test results showed that the bar bond stress was increased as the strain rate increased, and the required bar development length under high-strain rate was smaller than or equal to that under static load. Hwang et al. (2019a) conducted drop hammer test on RC beams having longitudinal bars partially bonded at the beam ends to investigate the effects of bar diameter, development length, drop height, and hammer mass on the bond strength. The test result also confirmed the increase of bond strength under high-strain rate, and a dynamic increase factor was proposed based on the strain rate effect of tensile strength of concrete to evaluate the bar development length in existing design methods. Jacques and Saatcioglu (2019a, 2020) performed beam-end tests and lap splice tests under high strain rates of $0.1\text{--}1.0 \text{ s}^{-1}$, and reported that the bond strength increased by 28–47%. However, the shape of the bond stress-slip curve was not significantly affected by high strain rates. Panteki et al. (2017) performed finite element analysis to investigate the dynamic bond behavior of pull-out test specimens under drop hammer load. Jacques and Saatcioglu (2019b) proposed an analytical model to consider the effect of high strain rates on the bar-slip in tension lap splices. Despite the advanced investigation for the required bar development length, the existing studies were mostly limited on simply pull-out test or modified beam-end test. To investigate the effect of impact load on the bond strength in actual situation, widely used lap splice test needs to be performed under impact load.

In the present study, drop hammer test was performed on twenty-four RC beams with lap sliced bars. The bar development length was designed to be shorter than the requirement of current design codes under static load. The test parameters were drop heights, hammer mass, bar diameter, and splice length. The structural performances including the impact force, deflection, failure mode, and strain of reinforcing bar were evaluated. The test result was compared with the energy-based non-linear analysis result addressing the dynamic effect of

materials. Further, a modification method was proposed to estimate the bar development length under impact load, addressing the strain rate effect of materials, impact damage, and impact energy loss.

2 Test Program

2.1 Test Specimens

Figure 1 and Table 1 show the test parameters of twenty-four RC beam specimens in detail. The cross-sectional area of the beam was $250 \text{ mm} \times 300 \text{ mm}$, the length was 2400 mm , and the span was 2000 mm . The test parameters were the diameter of longitudinal bars (i.e., D18 bar or D25 bar), splice length (i.e., 300 mm or 400 mm), hammer mass (i.e., 272.3 kg , 597.3 , or 857.3 kg), and drop height (i.e., 1.58 m to 12.60 m). The RC beam specimens were divided into four groups according to combination of the bar diameter and splice length. In the specimen name, the first letter S indicates bar splices, the first numbers 18 and 25 indicate bar diameter, and the second numbers 300 and 400 indicate splice length of reinforcing bars. The last letter L, if present, indicates additional two groups under different drop mass and height. Each group consisted of four identically designed RC beams under four different impact loading conditions. In specimen groups S-18-300-L and S-18-400-L, a mass of 272.3 kg was dropped at heights of 3.15 , 6.30 , and 12.60 m , and a 597.3 kg mass was dropped at a height of 5.47 m (i.e., the same impact energy of the mass of 272.3 kg dropped at a height of 12.60 m). In specimen groups S-18-300 and S-25-300, a mass of 532.3 kg was dropped at heights of 1.58 , 3.15 , and 4.73 m , and an 857.3 kg mass was dropped at a height of 1.96 m (i.e., the same impact energy of the mass of 532.3 kg dropped at a height of 3.15 m). In specimen groups S-18-400 and S-25-400, a mass of 532.3 kg was dropped at heights of 1.58 , 3.15 , and 6.30 m , and an

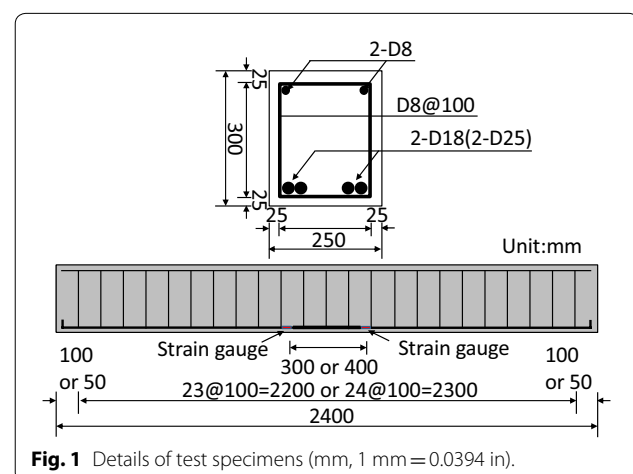


Fig. 1 Details of test specimens (mm, 1 mm = 0.0394 in).

Table 1 Summary of test program.

Specimen groups	Dimensions (mm × mm)	Longitudinal bars	Transverse bars	Splice length (mm)	Concrete strength (MPa)	Hammer mass (kg)	Drop height (m)	P_s/P_M
S-18-300-L	250 × 300	D18	D8@100	300	37.72	272.3	3.15/6.30/12.60	2.38
S-18-400-L				400	37.96	272.3	5.74	2.38
S-18-300				300	31.16	532.3	1.58/3.15/4.73	2.34
S-18-400				400	30.01	532.3	1.96	2.34
S-25-300		D25		300	34.62	532.3	1.58/3.15/4.73	1.38
S-25-400				400	32.77	532.3	1.96	1.38
						857.3	1.58/3.15/6.30	
						857.3	1.96	

P_s , shear resistance; P_M , flexural resistance; 1 kN = 0.2248 kips; 1 mm = 0.0394.

857.3 kg mass was dropped at a height of 1.96 m (i.e., the same impact energy of the mass of 532.3 kg dropped at a height of 3.15 m).

In specimens, four D18 bars (diameter = 18 mm, cross-sectional area = 254.5 mm², and rib height and width = 1.6 mm and 1.0 mm at a spacing of 10.0 mm) or four D25 bars (diameter = 25 mm and cross-sectional area = 490.9 mm², and rib height and width = 2.1 mm and 1.5 mm at a spacing of 12.5 mm) were used for lap spliced bottom longitudinal bars (i.e., reinforcing bar ratio = 1.58% for D18 bars or 3.09% for D18 bars). D8 bars (diameter = 8 mm and cross-sectional area = 50.3 mm²) were used for transverse bars at a spacing of 100 mm to prevent shear failure (i.e., static shear-flexural capacity ratio P_s/P_M was greater than 1.0 according to the calculation of ACI 318-19 (2019)). The splice lengths of 300 mm and 400 mm were 31 to 69% shorter than static requirements specified in ACI 318-19 (2019) (i.e. 578 mm for D18 bar and 955 mm for D25 bar, respectively). Concrete cover from the beam side (c_{so}) and bottom face (c_b) to the most external bar surface were 25 mm, and the clear space ($2c_{si}$) between spliced bars were 112 mm for D18 bar and 84 mm for D25 bar, respectively.

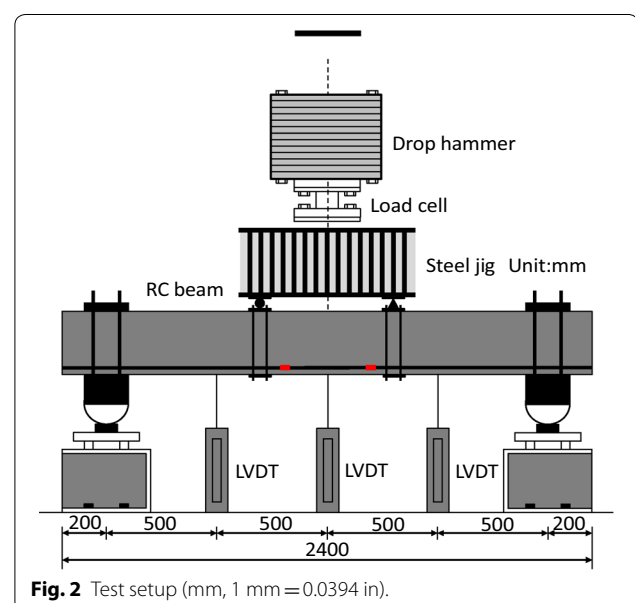
2.2 Materials

The mix proportion of ready-mixed concrete used to cast the RC beams in weight was 1.0: 0.6: 1.6: 2.8 for cement: water: fine aggregate: coarse aggregate. The aggregates used had a maximum size of 20 mm. Standard concrete cubes, 100 mm × 100 mm × 100 mm, were cast and tested to estimate the average concrete compressive strength according to ASTM (2018). According to Eurocode 2 (2004), concrete cylinder strength can be estimated

as 0.8 times concrete cube strength. At the day of impact loading test, concrete cylinder strength f'_c was from 30.01 to 37.96 MPa (refer to Table 1). In this study, the cylinder strength was used in the prediction of bar development length and numerical analysis. The yield strength f_y and tensile strength f_u of reinforcing bars were 497 MPa and 651 MPa for D18 bar, 469 MPa and 609 MPa for D25 bar, and 693 MPa and 883 MPa for D8 bar, respectively.

2.3 Test Setup and Instrumentation

Figure 2 shows the drop hammer test setup for RC beam specimens under impact load. To prevent uplifting of



specimens from pin supports, specimens were fixed in the vertical and horizontal directions at the pin supports. To apply four-point loading to specimens for lap splice test, a steel jig with a mass of 580.7 kg was installed on the top of the specimens. At each test, one impact load was applied to the steel jig on each specimen. The striking head of the drop hammer had a flat shape with a radius of 100 mm. Impact force was measured by a load cell attached to the head of the drop hammer. Reaction force was not measured due to the limited test setup. Using linear variable differential transformers (LVDTs), mid-span deflection was measured at the steel plates extruded from the beam side addressing concrete damage at the beam bottom. Strains of reinforcing bars were measured by uniaxial strain gauge at the end of lap splice length. A digital signal acquisition system with a sampling rate of 500 kHz was used to measure test data.

3 Test Results

3.1 Impact Force

Figure 3 shows the impact force–time relationships of test specimens. Table 2 lists the peak impact force (P_p). The impact force variation showed an initial pulse-like wave with high amplitude having extremely short duration and a wave with low amplitude having relatively longer duration (Hughes and Beeby 1982; Kishi et al. 2001; Ishikawa et al. 2002). Under the same hammer mass, as the drop height increased, the peak impact force increased. In the case of the same impact energy, heavier hammer mass (i.e., lower drop height) decreased the impact force (Fig. 3a, c or Fig. 3b, d). When the bar splice length increased, the peak impact force was not significantly increased (Fig. 3a, b or c, d). Further, the peak impact force was not affected by bar diameter (i.e., bar reinforcement ratio) (Fig. 3c, e or d, f). In other words, when the same hammer mass and drop height were used, the peak impact force discrepancy between the specimens having different bar splice length was insignificant, showing the average difference of 2.5%. It is noted that all test data of specimen S-25-300 under 1.96 m drop height was not measured due to the malfunction of trigger device for releasing the hammer.

3.2 Mid-span Deflection

Figure 4 shows the mid-span deflection-time relationships of test specimens. Table 2 lists the peak (δ_{test}) and residual (δ_r) mid-span deflections. The peak mid-span deflection increased as the drop height increased. However, unlike the impact force, the heavier hammer mass (i.e., lower drop height) at the same impact energy increased the mid-span deflection (Fig. 4a, c or b, d). When the bar splice length increased, the mid-span deflection decreased (Fig. 4a, b or c, d). The

larger reinforcement ratio (i.e., the larger bar diameter) improved the impact resistance, which decreased the mid-span deflection (Fig. 4c, e). However, at the drop heights of 1.96 and 6.30 m, the peak deflection of specimen S-25-400 was larger than that of S-18-400 due to significant local damage (Fig. 4d, f). The residual deflection of all specimens was larger than zero, showing inelastic behavior, which showed the same tendency with the peak deflection in accordance with the test parameters.

3.3 Failure Modes

Figure 5 shows the failure modes of specimens at the end of the test. In specimen group S-18-300-L, flexural cracks were propagated from the beam bottom toward the top (Fig. 5a). Cover concrete spalling occurred along the bar splice length at the drop height of 3.15 m. As the drop height increased, the length of cover concrete spalling zone and the width of vertical cracks increased, and diagonal cracks were concentrated to the loading points. In the beam specimen under 12.60 m drop height, vertical cracks were developed in the entire cross-section of the beam. In the case of the same impact energy, the heavier hammer mass increased the impact damage (Fig. 5a, c or b, d). This is because impact load due to heavier mass decreases impact energy loss, which increases impact damage of specimens (See 4.1). The longer bar splice length reduced the impact damage and cover concrete spalling due to the improved bond resistance (Fig. 5a, b).

In contrast, the larger bar diameter decreased the bond resistance, which increased the cover concrete spalling length and vertical crack width (Fig. 5c, e or d, f). Particularly, specimen S-25-400 under 6.30 m drop height showed the largest impact damage, and ultimately collapse occurred due to large bond failure. Except specimen S-18-400-L under 3.15 m drop height, failure mode was governed by cover concrete spalling in lap splice length, which directly decreased the bar bond strength.

As shown in Fig. 6, the bar bond stress is developed by the confinement of cover concrete and transverse bars. When impact load is applied to bar splice region, the impact force is transferred to the beam bottom, which causes cover concrete spalling along the bar splice length. Ultimately, the bar bond strength decreases, and the load-carrying capacity is significantly decreased by bond failure.

3.4 Reinforcing Bar Strain

Figure 7 shows strain variation of reinforcing bars at the end of lap splice length. Table 2 lists the peak strain (ϵ_u) and residual strain at 0.2 s (ϵ_r). In specimen group of S-18-300-L, as the drop height increased, the peak and residual strains of reinforcing bars increased (Fig. 7a). Further, the peak strain was greater than the yield

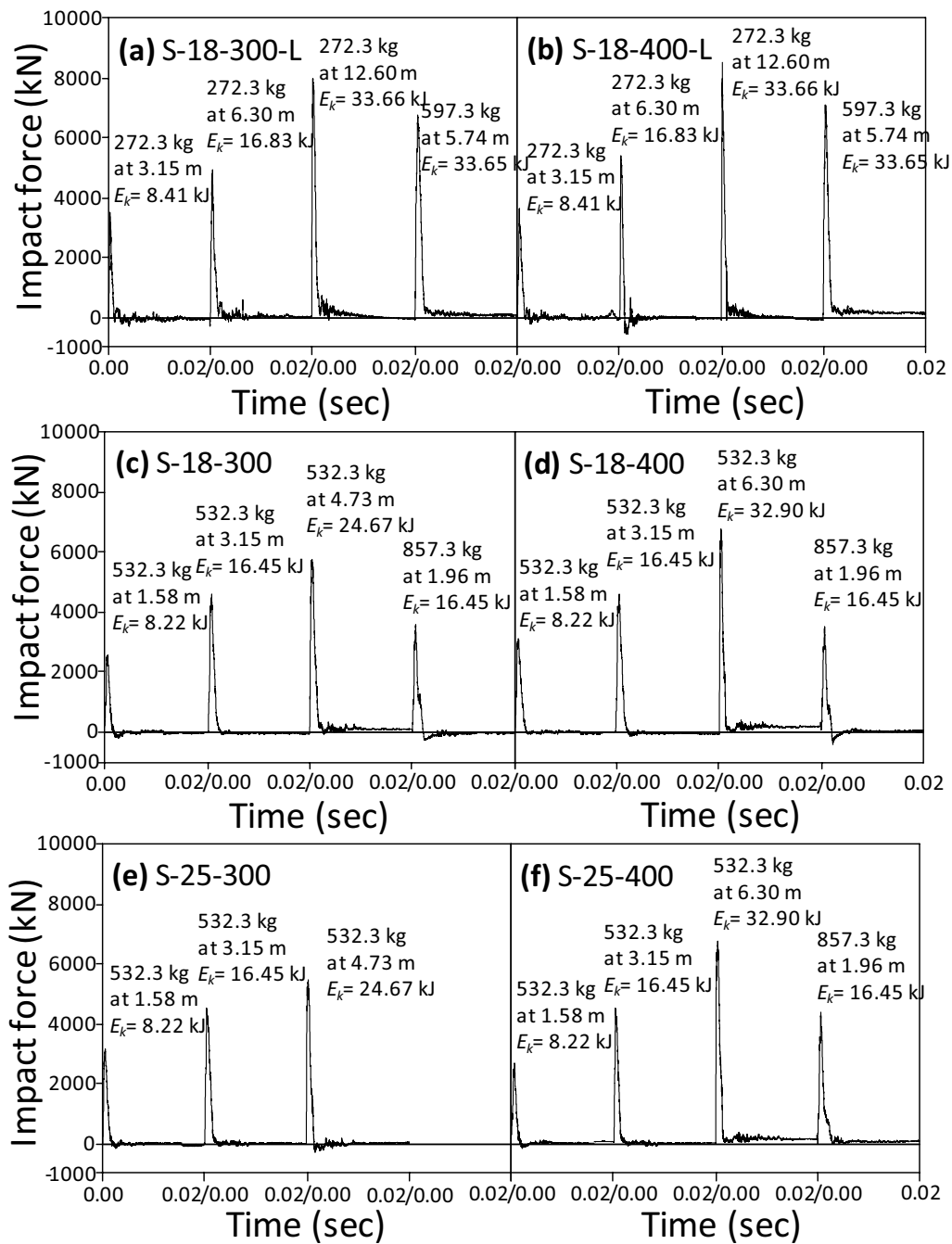


Fig. 3 Impact force history.

strain (=0.00249) and dynamic yield strain (=0.00282–0.00285 mm/mm in the drop heights). It is noted that the dynamic yield strain was calculated from the analysis results (refer to the chapter of “Deformation Energy E_d ”). This result indicates that longitudinal bars can be yielded under large impact load even though the bar

splice length is shorter than the requirement under static load.

In specimen group S-18-300 with the lower drop height and heavier hammer mass, however, the peak strain was smaller than the dynamic yield strain (=0.00283–0.00284 mm/mm) due to early bond failure (Fig. 7c). This is because the reduced impact velocity decreases

Table 2 Summary of test result.

Specimens	Drop height (m)	Drop weight (kg)	Impact energy (kJ)	P_p (kN)	δ_p (mm)	δ_r (mm)	ε_u (10^{-6} mm/mm)	ε_r (mm/mm)	Strain rate (1/s)
S-18-300-L	3.15	272.3	8.41	3518	23.1	18.3	1280	450	2.91
	6.30	272.3	16.83	4953	86.6	75.6	2140	1680	4.14
	12.60	272.3	33.66	8002	165.6	151.7	3070	1760	5.30
	5.74	597.3	33.65	6771	194.6	176.1	3100	1950	5.93
S-18-400-L	3.15	272.3	8.41	3622	12.8	5.8	1600	380	2.91
	6.30	272.3	16.83	5380	60.5	50.6	2150	540	4.15
	12.60	272.3	33.66	8566	150.9	138.0	3140	1370	5.31
	5.74	597.3	33.65	7108	167.0	159.0	3360	1580	5.93
S-18-300	1.58	532.3	8.22	2540	55.8	52.4	1610	320	3.19
	3.15	532.3	16.45	4588	101.7	88.7	2160	1370	4.11
	4.73	532.3	24.67	5716	159.6	144.9	2570	840	4.97
	1.96	857.3	16.45	3590	137.7	135.2	2430	1380	4.16
S-18-400	1.58	532.3	8.22	3123	38.9	34.7	2030	340	3.16
	3.15	532.3	16.45	4589	83.2	77.8	2210	680	4.09
	6.30	532.3	32.90	6768	183.2	167.0	3430	1130	5.61
	1.96	857.3	16.45	3541	104.0	100.0	2540	1050	4.14
S-25-300	1.58	532.3	8.22	3140	32.4	30.2	1690	240	2.80
	3.15	532.3	16.45	4500	95.2	89.8	2170	1360	3.53
	4.73	532.3	24.67	5484	134.8	118.1	3320	780	4.26
	1.96	857.3	16.45	–	–	–	–	–	–
S-25-400	1.58	532.3	8.22	2685	23.5	15.1	2070	320	2.75
	3.15	532.3	16.45	4500	75.0	72.3	2290	8970	3.49
	6.30	532.3	32.90	6768	193.8	185.2	3470	1520	4.70
	1.96	857.3	16.45	4410	122.8	118.4	2580	320	3.52

Impact energy was calculated from potential energy of mgh (i.e. m drop weight; g gravity acceleration 9.81 m/s^2 ; and h = drop height). Strain rate was calculated from the energy based method and section analysis.

the strain rate effect on the bar bond strength, while the heavier drop mass increases the impact damage.

When the bar splice length increased, the peak strain increased (S-18-300-L compared with S-18-400-L, S-18-300 compared with S-18-400, or S-18-400 compared with S-18-400). On the other hand, the peak strain of D25 bar was comparable to that of D18 bar at the same bar splice length and impact energy (S-25-300 compared with S-18-300, or S-25-400 compared with S-18-400). In the case of the same impact energy, the heavier drop mass (i.e., lower drop height) increased the peak strain.

High strain rate effect due to impact force increases concrete strength and causes the stress concentration on the bar splice end during extremely short time. For this reason, the peak strain of the bar splices can be greater than the dynamic yield strain.

4 Evaluation of Structural Performance Under Impact Load

High strain rate increases the material properties of concrete and reinforcing bars, which increases the load-carrying capacity of RC beams subjected to impact load (Wakabayashi et al. 1980; Kulkarni and Shan 1998; Li et al. 2000; Li et al. 2011). As shown in Figs. 3, 4, 5, 6, 7, although early bond failure was estimated by the observation in the test, longitudinal bars yielded. To assure the bond failure mode in the specimens, the peak deflection of RC beams was evaluated by modifying the Hwang et al. (2019) method.

4.1 Energy Conservation Model

In the Hwang et al. (2019b) method, an energy conservation law between the impact energy and resistant energy was used, which assumed: (1) perfect bond between reinforcing bars and concrete; (2) before collision, the drop hammer with an initial velocity V_i has the kinetic energy E_k ; (3) during collision, the kinetic energy E_k is converted into the impact damage and deflection δ of the RC beam;

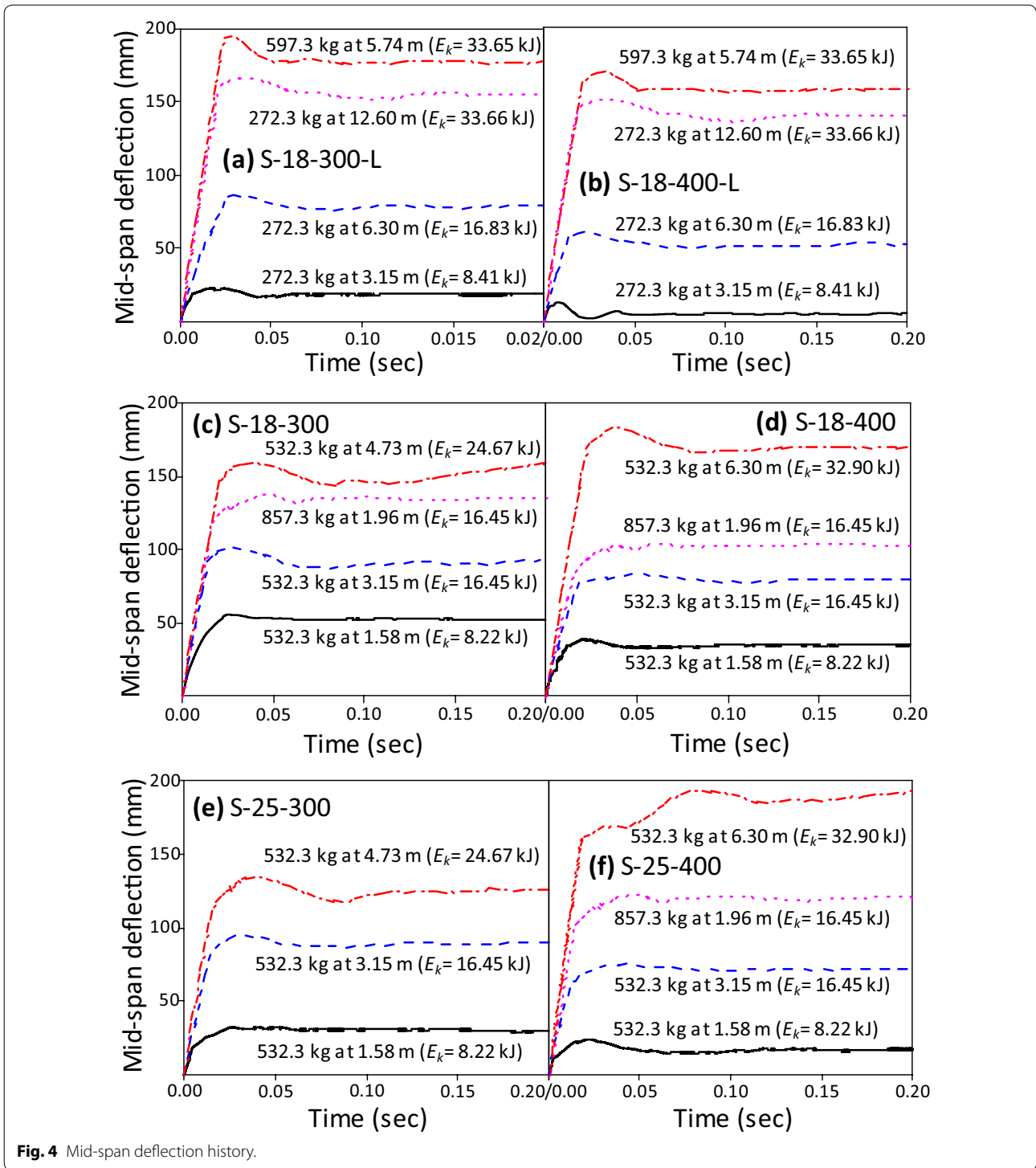


Fig. 4 Mid-span deflection history.

(4) after collision, the RC beam with steel jig and dropped mass move together with the same velocity V_c based on a perfectly plastic collision (Suzuki et al. 1996); and (5) the potential energy E_p due to the deflection δ after collision causes additional damage and deflection. In the energy

conservation equation, the impact energy E_k and potential energy E_p are dissipated by the deformation energy E_d of the RC beam, spalling energy E_s of cover concrete, and energy loss E_l due to the energy transformed from the drop hammer to the RC beam (Hwang et al. 2019).

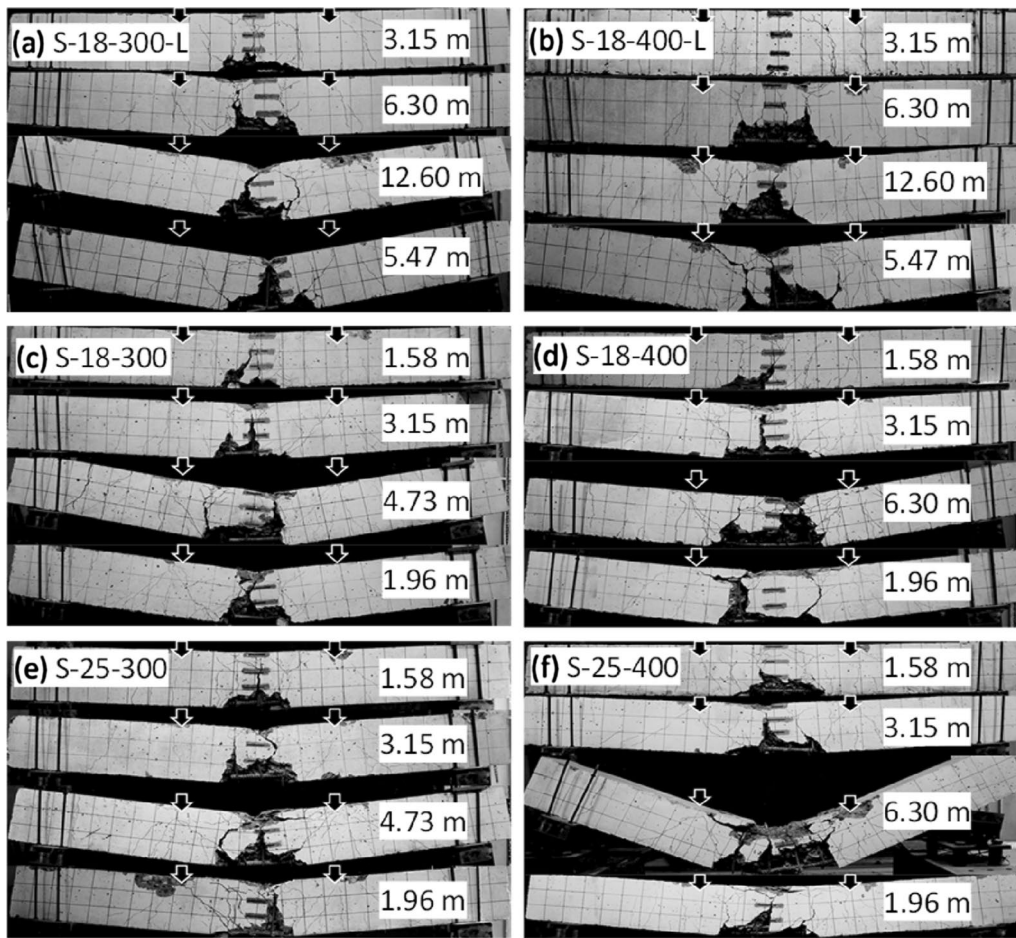


Fig. 5 Failure modes at the end of tests.

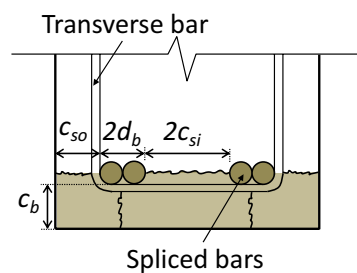


Fig. 6 Reduced confinement of cover concrete under impact load.

$$E_k + E_p = E_d + E_s + E_t \tag{1}$$

where the definition of each energy is listed in Table 3.

4.2 Deformation Energy E_d

To estimate the deformation energy E_d , a load-deflection relationship of the RC beam should be defined. Fiber

analysis method (Spacone and EI-Tawil 2004) was used considering the perfect bond between concrete and longitudinal bars, strain compatibility at the cross-section, confinement effect of transverse bars, and dynamic material properties due to high strain rate. Figure 8 shows the curvature distribution of a simply supported RC beam subjected to four-point loading. The curvature ϕ at the mid-span can be calculated from the mid-span deflection δ (Ou and Nguyen 2014).

$$\phi = \frac{24}{3L^2 - 4L_s^2} \delta \text{ for } 0 \leq \delta \leq \delta_y \tag{2a}$$

$$\phi = \phi_y + \frac{1}{L_p(L_s - 0.5L_p)} (\delta - \delta_y) \text{ for } \delta > \delta_y \tag{2b}$$

where L = beam span; L_s = shear span; L_p = plastic hinge length; δ_y = yield deflection; and ϕ_y = yield curvature.

Figure 9 shows the linear strain distribution at the beam section in the mid-span. Using the curvature ϕ ,

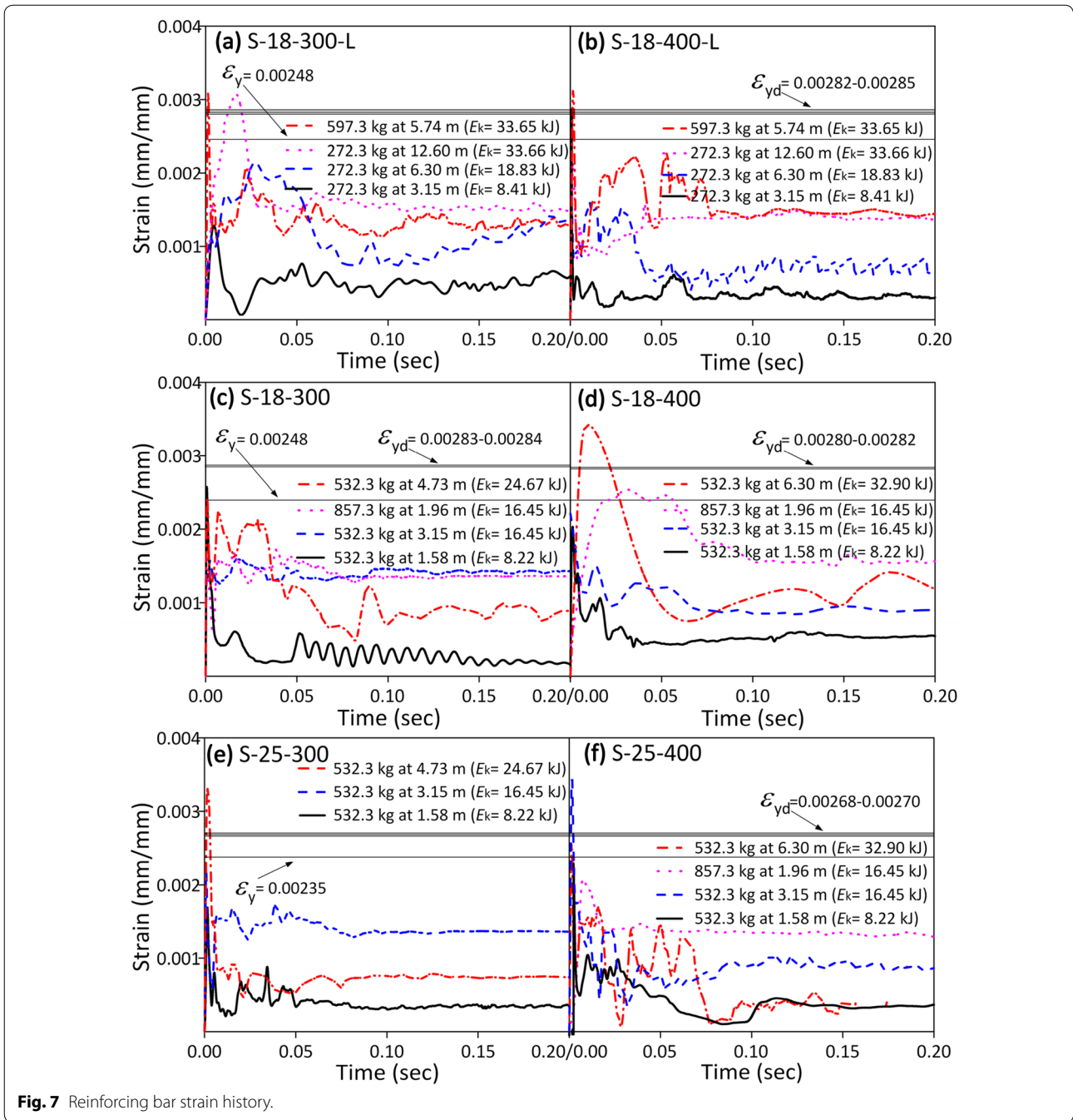


Fig. 7 Reinforcing bar strain history.

the strain ϵ_i at each fiber element can be determined as follows.

$$\epsilon_i = (y_0 - y_i)\phi \tag{3}$$

where y_i =distance from the extreme compression fiber to the centroid of each fiber element; and y_0 =distance from the extreme compression fiber to the neutral axis.

Under impact load, the strain rate effect on the material properties should be considered. In this study, the strain rate effects specified in CEB (1988) and *fib* 2010 (2010) were considered for reinforcing bars and concrete, respectively (refer to Table 4). The strain rate at each fiber element can be defined as a linear function of curvature rate $\dot{\phi}$ (Fujikake et al. 2009).

Table 3 Equations of each energy for energy conservation law.

Energy types	Equations
Kinetic energy E_k	$E_k = 0.5m_h V_i^2 = m_h g h_d$
Potential energy E_p	$E_p = \begin{cases} (m_{be} + m_h)g\delta & \text{for } \delta < \delta_y \\ (m_{be} + m_h)g\delta + (m_{bp} + m_h)g(\delta - \delta_y) & \text{for } \delta > \delta_y \end{cases}$
Deformation energy E_d	$E_d = \int_0^\delta P(\delta)d\delta$
Spalling energy E_s	$E_s = \begin{cases} 0 & \text{for } \epsilon_c < \epsilon_{cu} \\ 0.2f_{td}bc_c k_s (L_p + 2C_c) & \text{for } \epsilon_{cs} < \epsilon_{yd} \\ k_s = (300/h)^{0.25} \leq 1 \end{cases}$
Energy loss E_l	$E_l = E_k - \frac{1}{2}(m_{be} + m_h)V_c^2 = \frac{m_{be}}{m_{be} + m_h} E_k$

m_h , drop hammer mass; g , acceleration of gravity ($=9.81$ m/s); h_d , drop height; m_{be} and m_{bp} , equivalent masses of the RC beam showing elastic and plastic deflections ($=0.52m_b + m_j$ and $0.56m_b + m_j$) (Biggs 1964); m_b , mass of the beam; m_j , mass of the steel jig; δ_y , yield deflection; P , load due to beam moment; δ_{sp} , spalling deflection; ϵ_c , concrete compressive strain at extreme compression fiber; ϵ_{cu} , ultimate compressive strain of concrete; ϵ_{cs} , compression bar strain; ϵ_{yd} , dynamic yield strain of reinforcing bar; f_{td} , dynamic concrete tensile strength; b , beam width; c_c , concrete cover; k_s , size effect factor; L_p , plastic hinge length ($=0.5d + 0.05L_s$) (Mattock 1967); d , effective beam depth; L_s , shear span.

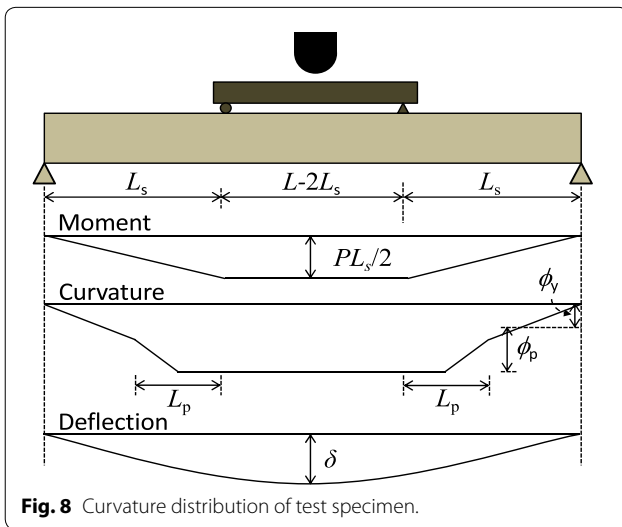


Fig. 8 Curvature distribution of test specimen.

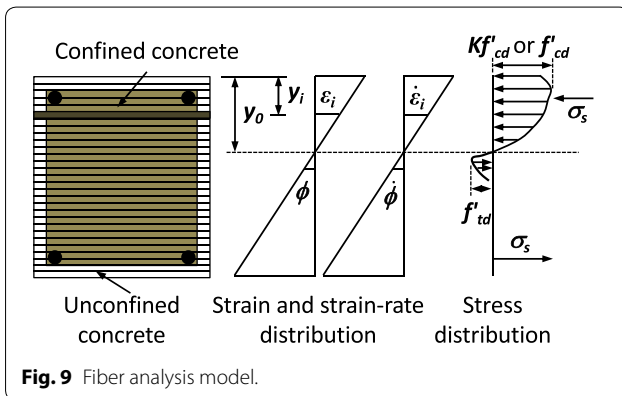


Fig. 9 Fiber analysis model.

$$\dot{\epsilon}_i = |(y_0 - y_c)|\dot{\phi} \tag{4}$$

On the basis of Eq. (2), the curvature rate $\dot{\phi}$ can be defined as a function of the mid-span deflection rate $\dot{\delta}$ (=velocity V_c at collision) (Hwang et al. 2019; Fujikake et al. 2009).

$$\dot{\phi} = \frac{24}{3L^2 - 4L_s^2} \dot{\delta} \text{ for } 0 \leq \delta \leq \delta_y \tag{5a}$$

$$\dot{\phi} = \frac{1}{L_p(L_s - 0.5L_p)} \dot{\delta} \text{ for } \delta > \delta_y \tag{5b}$$

Figure 10 shows the stress–strain relationship of reinforcing bars and concrete. Bilinear curve was used for reinforcing bars, and Kent and Park model (Kent and Park 1971; Scott et al. 1982) was used for concrete. The detailed constitutive models of reinforcing bar and concrete are defined in Table 4.

The deflection δ is estimated as follows: (1) the curvature rate and strain rate are calculated from Eqs. (4) and (5), respectively; (2) on the basis of the dynamic stress–strain relationships for reinforcing bars and concrete, nonlinear numerical analysis is performed (Table 4); (3) the deflection δ is determined (Eq. (2)); (4) each energy is calculated (Tables 3); and (5) the maximum deflection is determined satisfying Eq. (1).

4.3 Mid-span Deflection of RC Beam Under Impact Load

Table 5 compares the prediction of Eq. (1) to the measured peak deflection. In the present study, as the dropped mass collided on the RC beam indirectly, the spalling energy E_s was neglected according to the failure mode in the specimens (Fig. 5). The prediction assuming the perfect bond between reinforcing bars and concrete δ_p was less than the test result δ_{test} , showing the average value of $\delta_p/\delta_{test} = 0.38$ and $COV. = 0.47$. This result implies that bond failure occurred in all specimens under impact load (except S-18-400-L under 3.15 m drop height). Thus, the contribution of bar bond-slip to the deflection needs to be considered. In specimen S-18-400-L under 3.15 m drop height, on the other hand, the prediction agreed well with the test result ($\delta_p/\delta_{test} = 1.07$), showing flexural failure without bond failure. This result coincided with the actual failure mode in the test.

5 Prediction for Bar Development Length

5.1 Existing Methods for Bar Development Length

Existing design methods for the bar development length under static load are listed in Table 6. The tensile stress f_s of bar splices was calculated from the design development length l_d . Considering the condition of lap splice used in the test specimens, the development length l_d was

Table 4 Constitutive models for reinforcing bar and concrete.

Materials	Stress-strain relationship	Strain rate effect
Reinforcing bar	$\sigma_s = \begin{cases} E_s \varepsilon_s & \text{for } \varepsilon_s \leq \varepsilon_{yd} \\ f_{yd} + E_h (\varepsilon_s - \varepsilon_{yd} < 1.25 f_{yd}) & \text{for } \varepsilon_s > \varepsilon_{yd} \end{cases}$	$f_{yd} = f_y + 6 \ln(10^5 \dot{\varepsilon} /5) \leq f_y + 6 \ln(2 \times 10^5)$ (CEB)
Confined concrete under compression	$\sigma_{cc} = \begin{cases} kf'_{cd} \left[\frac{2\varepsilon_c}{\varepsilon_{cod}K} + \left(\frac{\varepsilon_c}{\varepsilon_{cod}K} + 1 \right)^2 \right] & \text{for } \varepsilon_c \geq -\varepsilon_{cod}K \\ kf'_{cd} [1 + Z_m (\varepsilon_c + \varepsilon_{cod}K)] \geq 0.2f'_{cd} & \text{for } \varepsilon_c < -\varepsilon_{cod}K \end{cases}$ $K = 1 + \rho_t f_{yt} / f'_{cd}$ $Z_m = \frac{0.5}{\frac{3+0.29f'_{cd}}{145f'_{cd}-1000} + \frac{3}{4} \rho_t \sqrt{\frac{h_0}{s}} - \varepsilon_{cod}K}$	$f'_{cd} = \begin{cases} f'_c (10^5 \dot{\varepsilon}/3)^{0.014} & \text{for } \dot{\varepsilon}_c < 30/s \\ 0.012 f'_c (10^5 \dot{\varepsilon}/3)^{0.1/3} & \text{for } \dot{\varepsilon}_c \geq 30/s \end{cases}$ (fib2010)
Unconfined concrete under compression	$\sigma_{cu} = f'_{cd} \left[\frac{2\varepsilon_c}{\varepsilon_{cod}} + \left(\frac{\varepsilon_c}{\varepsilon_{cod}} \right)^2 \right]$ for $-\varepsilon_{cu} \leq \varepsilon_c \leq 0$	
Concrete under tension	$\sigma_t = E_{cd} \varepsilon_c, 0 < \varepsilon_c \leq f'_{td} / E_{cd}$	$f'_{td} = \begin{cases} f'_c (10^6 \dot{\varepsilon})^{0.018} & \text{for } \dot{\varepsilon}_c < 10/s \\ 0.0062 f'_c (10^6 \dot{\varepsilon})^{1/3} & \text{for } \dot{\varepsilon}_c \geq 10/s \end{cases}$ (fib2010)
		$f_t = \begin{cases} 0.3 f'_c{}^{2/3} & \text{for } f'_c < 50 \text{MPa} \\ 2.12 \ln[1 + 0.1(f'_c + 8)] & \text{for } f'_c \geq 50 \text{MPa} \end{cases}$ (fib 2010)

σ_s , reinforcing bar stress; f_{yd} and f_y , dynamic and static yield strength of reinforcing bar; ε_{yd} , dynamic yield strain of reinforcing bar; E_s and E_h , elastic and strain hardening moduli ($E_h = 0.01E_s$); σ_{cc} and σ_{cu} , stress of confined concrete and unconfined concrete in compression; f'_{cd} and f'_c , dynamic and static compressive strength of concrete; ε_{cod} and ε_{c0} , dynamic and static peak strain ($= \varepsilon_{cod} (10^5 \dot{\varepsilon}_c / 3)^{0.02}$ and $0.0006 + 0.005 \ln(f'_c)$, respectively) (fib 2010); f_{yt} , yield strength of transverse bars; ρ_t , volumetric ratio of transverse bars ($= 2A_t(h_{ix} + h_{iy}) / (h_{ox}h_{oy}s)$); A_t , sectional area of transverse bars; h_{ix} and h_{iy} , center-to-center distances of transverse bars in x- and y- directions; h_{ox} and h_{oy} , outer distances of transverse bars in x- and y- directions; and s , spacing of transverse bars; ε_{cu} , ultimate compressive strain corresponding to $0.2f'_{cd}$ (Scott et al. 1982); σ_t , concrete stress in tension; E_c and E_{cd} , static and dynamic elastic modulus ($= 21500 \sqrt[3]{f'_c} / 10$ and $E_c (10^5 \dot{\varepsilon}_c)^{0.026}$, respectively) (fib 2010); f_{td} and f_t , dynamic and static tensile strength of concrete.

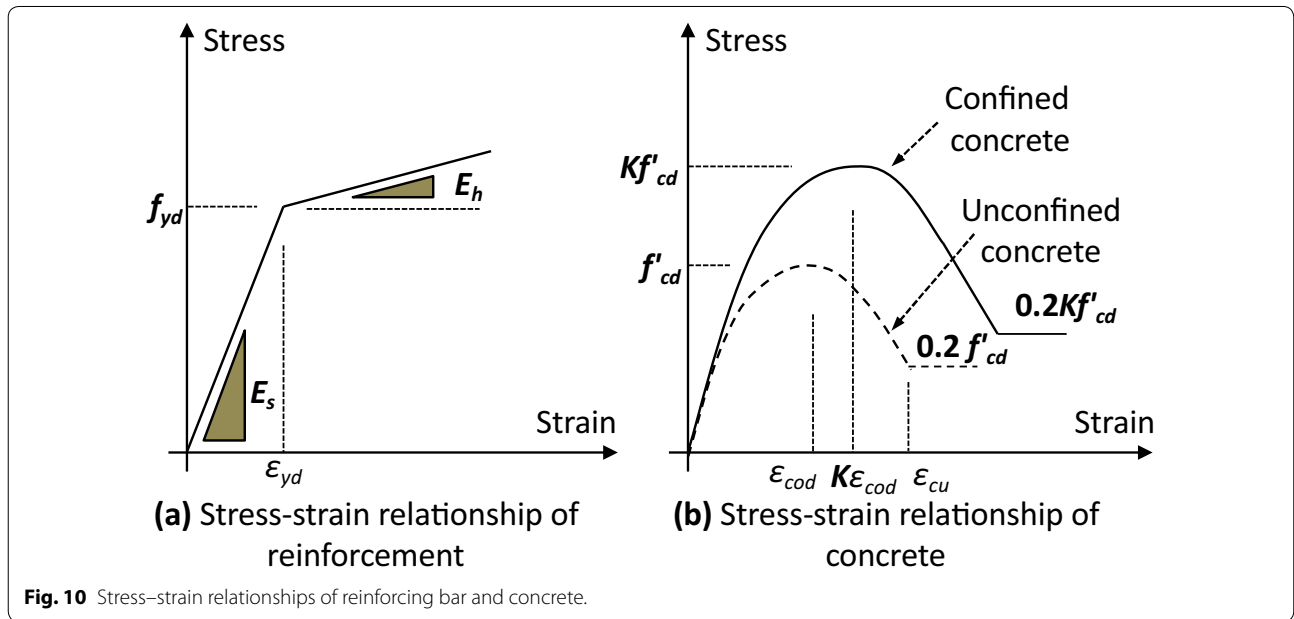


Fig. 10 Stress–strain relationships of reinforcing bar and concrete.

defined as $l_d = l_{sp} / 1.3$ for ACI 318-19 (2019), $l_d = l_{sp} / 1.5$ for Eurocode 2 (2004), and $l_d = l_{sp}$ for ACI 408-03 (2003) and Hwang et al. (2017) method, where l_{sp} = lap splice length. Further, safety factors were not considered in the calculation of f_s for direct comparison with the test results.

Figure 11 compares the test results f_{test} with the bar stress predictions f_s of the existing design codes including

ACI 318-19 (2019), ACI 408-03 (2003), and Eurocode 2 (2004), and Hwang et al. (2017) method without consideration of the strain rate effect (i.e., static load). It is noted that the effect of bar diameter on the bond strength was neglected on the basis of the test result (e.g., S-18-300 compared with S-25-300, or S-18-400 compared with S-25-400 in Table 2). Thus, the coefficient of bar diameter $\psi_s = 1.0$ for ACI 318-19 (2019) and ACI 408-03

Table 5 Comparison of peak deflection in test with predicted deflection.

Specimens	Drop height (m)	Drop weight (kg)	δ_{test} (mm)	δ_p (mm)	δ_p/δ_{test}
S-18-300-L	3.15	272.3	23.1	13.8	0.60
	6.30	272.3	86.6	23.1	0.27
	12.6	272.3	165.6	42.0	0.25
	5.74	597.3	194.6	68.2	0.35
S-18-400-L	3.15	272.3	12.8	13.7	1.07
	6.30	272.3	60.5	23.1	0.38
	12.60	272.3	150.9	42.0	0.28
	5.74	597.3	167.0	68.1	0.41
S-18-300	1.58	532.3	55.8	19.3	0.35
	3.15	532.3	101.7	34.6	0.34
	4.73	532.3	159.6	49.7	0.31
	1.96	857.3	137.7	44.3	0.32
S-18-400	1.58	532.3	38.9	19.4	0.50
	3.15	532.3	83.2	34.8	0.42
	6.30	532.3	183.2	64.3	0.35
	1.96	857.3	104.0	44.5	0.43
S-25-300	1.58	532.3	32.4	13.0	0.40
	3.15	532.3	95.2	22.0	0.23
	4.73	532.3	134.8	31.2	0.23
	1.96	857.3	–	–	–
S-25-400	1.58	532.3	23.5	13.1	0.56
	3.15	532.3	75.0	22.2	0.30
	6.30	532.3	193.8	40.7	0.21
	1.96	857.3	122.8	28.0	0.23
				Avg.	0.38
			COV.	0.47	

(2003), $\eta_2=1.0$ for Eurocode 2 (2004), and $\alpha_d=1.0$ for the Hwang et al. (2017) method were used (Table 6). In the calculation, the bar stress prediction was less than the yield strength (i.e., $f_s \leq f_y$). In the case of non-yielded bars, the existing methods except for ACI 318-19 (2019) overestimated the bar stress of D18 bars, whereas those methods underestimated D25 bars despite the neglected bar diameter effect. In the case of yielded bars, the existing methods underestimated the bar stress in overall.

5.2 Effect of Impact Load

According to 3-point impact loading test results performed by Hwang et al. (2019), bar bond strength under impact load was increased by the high strain rate effect on concrete tensile strength. In specimens under 4-point impact load, however, the bond strength would be decreased by cover concrete damage along the bar development length. To evaluate the effect of impact load on the bar development length, followings were additionally considered: the high strain rate effect on the concrete tensile strength and yield strength of reinforcing bars

(i.e., dynamic yield strength); and concrete cover was neglected along the development length on the basis of failure mode in the test specimens (for simple calculation, the same concrete cover was considered regardless of impact load level). It is noted that the value of 0.1 mm (i.e., $C_b = C_{so} = 0.1$ mm) was used to avoid a calculation error in ACI 408-03 (2003) and Eurocode 2 (2004) (Table 6).

Under dynamic load, strength increment can be estimated by a dynamic increase factor (*DIF*), which is defined as the ratio of dynamic strength to static strength of materials. In the calculations of ACI 318-19 (2019), ACI 408-03 (2003), and Eurocode 2 (2004), the tensile strength f_{sd} of bar splices under impact load was increased by the value of *DIF* for concrete tensile strength.

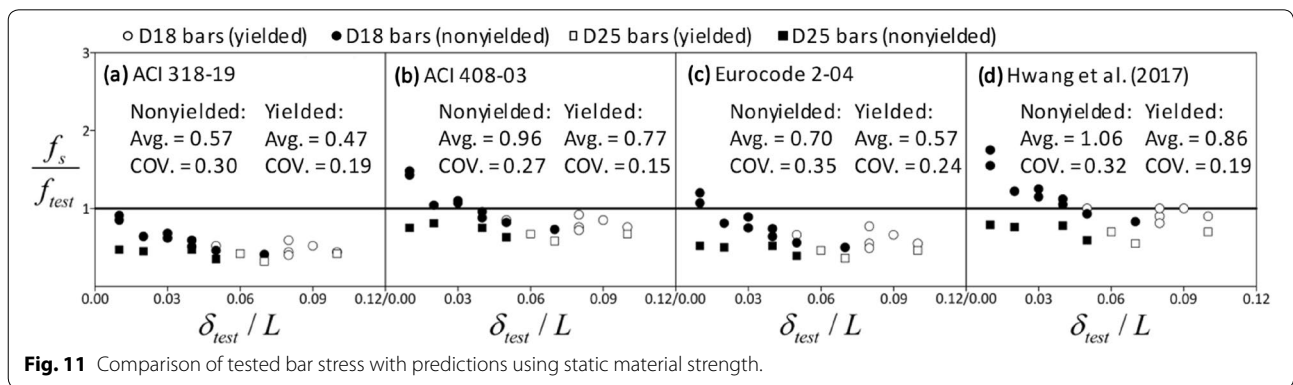
$$f_{sd} = DIF \times f_s = \frac{f_{td}}{f_t} \times f_s \leq f_{yd} \quad (6)$$

where f_{td} and f_t =dynamic and static tensile strength of concrete specified in *fib* (2010) (Table 4). In the Hwang

Table 6 Bar development length under static load.

Design methods	Development length (mm)		Splice length l_{sp}
ACI 318-19	$l_d = \frac{f_y d_b}{1.1 \lambda \sqrt{f'_c}} \frac{\psi_t \psi_e \psi_s}{(c_f + K_{tr})/d_b} \geq 300 \text{ mm}$	$(c_f + K_{tr})/d_b \leq 2.5$ $c_f = \min(c_b, c_{so}, c_{sj}) + 0.5d_b$ $K_{tr} = 40A_{tr}/(s_t n)$	1.0–1.3 l_d
ACI 408R-03	$l_d = \frac{(f_y/\sqrt{f'_c} - \phi 57.4w)(\psi_t \psi_e \psi_s) d_b}{\phi 1.83(cw + K_{atr})/d_b}$	$(cw + K_{atr})/d_b \leq 4.0$ $w = 0.1(c_{max}/c_{min}) + 0.9 \leq 1.25$ $K_{atr} = 6\sqrt{f'_c} t_d A_{tr}/(s_t n)$ $t_d = 0.03d_b + 0.22$ $c = c_{min} + d_b/2$ $c_{max} = \max(c_b, c_s)$ $c_{min} = \min(c_b, c_s)$ $c_s = \min(c_{so}, c_{sj} + 6.4)$	l_d
Eurocode 2-04	$l_d = \alpha_2 \alpha_3 \frac{f_y d_b}{4f_{bd}} \geq \frac{l_0}{1.5}$	$\alpha_2 = 0.7 \leq 1 - 0.15(c_d - d_b)/d_b \leq 1.0$ $\alpha_3 = 0.7 \leq 1 - K(\sum A_{tr} - A_s)/A_s \leq 1.0$ $f_{bd} = 2.25\eta_2 [0.75(0.3)(f'_c)^{2/3}]$ $\alpha_2 \alpha_3 \geq 0.7$ $c_d = \min(c_b, c_{so}, c_{sj})$ $l_0 = \max(0.45d_b f_y/(4f_{bd}), 15d_b, 200\text{mm})$ $\eta_2 = (132 - d_b)/100 \leq 1.0$	1.0–1.5 l_d
Hwang et al. (2017)	$f_s = \frac{l_d}{d_b} [3\tau_1 + \tau_2] \leq f_y$	$\tau_1 = \frac{\tau_u}{1.4} \left[\frac{1 - (\Delta f/s_1)^{1.4}}{1 - (\Delta f/s_1)} \right] \leq \tau_u$ $\frac{\Delta f}{s_1} = 1 - \frac{14.7l^2}{E_s d_b} \frac{\tau_u}{\sqrt{f'_c}} + 0.007 \frac{l_d}{\sqrt{f'_c}}$ $\tau_u = 0.91 \alpha_d \sqrt{f'_c} \left[\frac{(cw + K_{atr})/d_b}{2.5} \right]$ $\tau_2 = \left[\frac{16 - 6C_1 \tau_1}{16 + C_1 \tau_u} \right] \tau_u \geq \frac{\tau_u}{2}$ $C_1 = l_d^2/[1 - (\sqrt{0.003f'_c})E_s d_b]$	l_d

d_b is bar diameter; λ is coefficient of concrete type (= 0.75 to 1.0); ψ_t is coefficient of fresh concrete below the development length (= 1.0 to 1.3); ψ_e is coefficient of epoxy-coated bars (= 1.0 to 1.5); ψ_s is coefficient of bar diameter (= 0.8 to 1.0); c_b is thickness of the bottom cover concrete; c_{so} is the thickness of side cover concrete; c_{sj} is one-half of the center-to-center bar spacing; A_{tr} is total cross-sectional area of transverse bar within spacing s_t that cross the potential plane of splitting; n is the number of bars being developed or spliced along the splitting plane; and s_t is center-to-center distance of the transverse bars; ϕ is safety factor for structural design (= 0.82); K is coefficient of arrangement of the transverse bar (= 0 to 0.1); $\sum A_{tr}$ is total cross-sectional area of transverse bars within the development length; and A_s is the maximum cross-sectional area of the bar; η_2 is the coefficient of the diameter of the bar; α_d is coefficient related to reinforcing bar diameter (= 1.1 for D19 bars or less, 1.0 for D22 to D29 bars, and 0.9 for D32 bars or greater).



et al. (2017) method, the value of *DIF* was applied to the peak bond stress τ_u .

$$\tau_{ud} = DIF \times \tau_u = \left(\frac{f_{td}}{f_t} \right) \times 0.91 \alpha_d \sqrt{f'_c} \left[\frac{(cw + K_{atr})/d_b}{2.5} \right] \tag{7}$$

where α_d = coefficient related to reinforcing bar diameter; c and w = coefficients related to confinement cover concrete; and K_{atr} = coefficient related to confinement of transverse bars (Table 6).

Figure 12 compares the test results with the bar stress predictions considering the strain rate effect on concrete tensile strength and neglecting concrete cover. Because

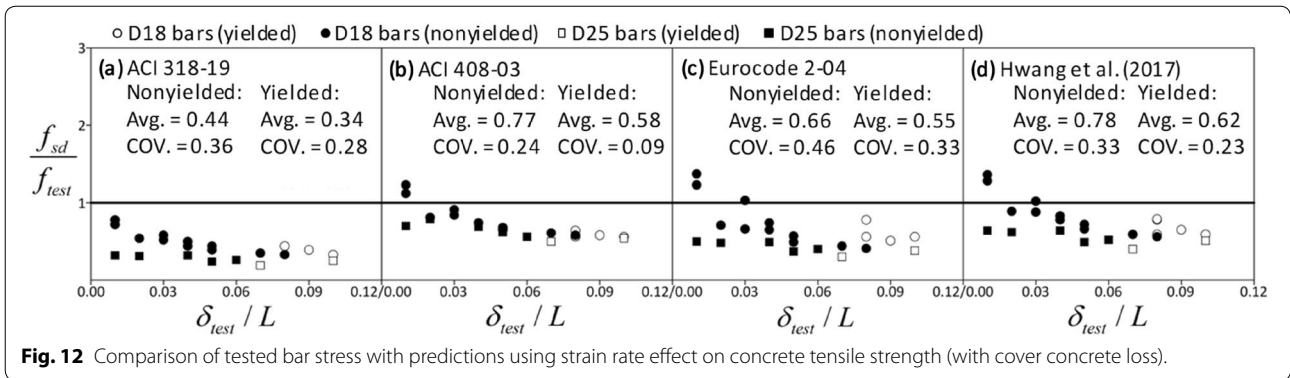


Fig. 12 Comparison of tested bar stress with predictions using strain rate effect on concrete tensile strength (with cover concrete loss).

the dynamic yield strength of a reinforcing bar cannot be directly measured from the test result, the numerical analysis was performed. The dynamic yield strength of the reinforcing bar was determined by multiplying the static yield strength by the increase ratio of 13.3–14.6%. The strain rate effect of materials increased the bond strength by 30.6–32.4%. Thus, the strain rate effect can decrease the bar development length to 13.9–16.8% (i.e., 1.306/1.146–1.324/1.133) of static state. However, cover concrete loss decreases the bond strength by 4.8–60.0% (i.e., 35.1–47.7% in ACI 318-19 (2019), 58.3–60.0% in ACI 408-03 (2003), 4.8%~12.5% in Eurocode 2 (2004) and 58.3–60.0% in Hwang et al. (2017) method), which requires the bar development length increased by 31.9–119.4% (i.e., 1.133/1.324/0.649–1.146/1.306/0.4 except Eurocode 2 (2004)) of static bar development length. In comparison with the predictions under static load, the proposed method (Eq. (7)) predicted the test results too conservatively, showing the average value=0.78 and 0.62, and COV.=0.33 and 0.23 for non-yielded and yielded bars in the Hwang et al. (2017) method, respectively. Particularly, as the peak deflection increased (i.e., larger impact energy), the predictions were underestimated. The other proposed methods based on existing design codes showed the same tendency.

As shown in Fig. 12, the tensile strength of bar splices was underestimated under large impact energy even though the same cover concrete loss was considered in all specimens. Further, when the same impact load was applied to beam specimens, the heavier drop mass (i.e., the lower impact energy loss) increased the bar strain (refer to Table 2). To improve the prediction accuracy, modification factors were additionally proposed for ACI 318-19 (2019), ACI 408-03 (2003), Eurocode 2 (2004), and the Hwang et al. (2017) method as follows.

$$f_{sdmg} = \frac{1}{0.87D_{mg} - 0.15} \times f_{sd} \leq f_{yd} \tag{9a}$$

for ACI 318-19

$$f_{sdmg} = \frac{1}{1.05D_{mg} + 0.04} \times f_{sd} \leq f_{yd} \tag{9b}$$

for ACI 408-03

$$f_{sdmg} = \frac{1}{2.10D_{mg} - 0.7} \times f_{sd} \leq f_{yd} \tag{9c}$$

for Eurocode 2-04

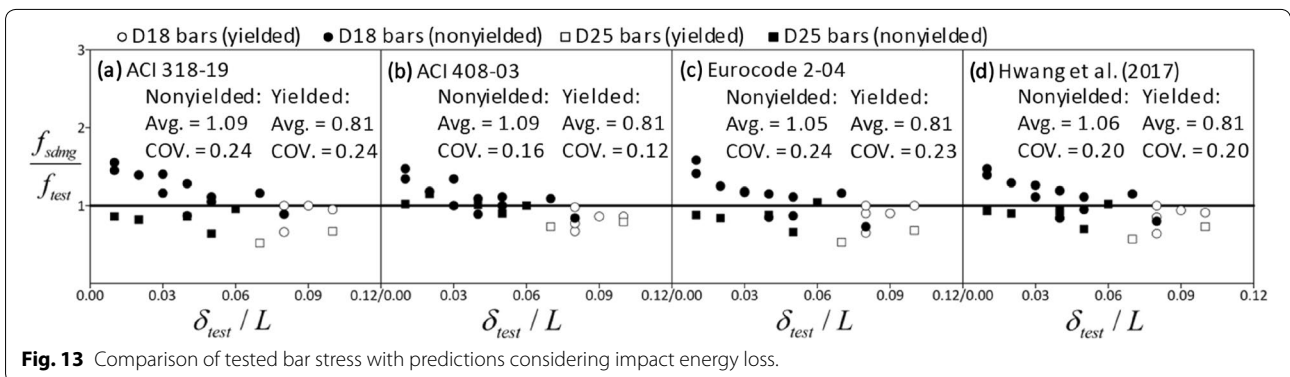


Fig. 13 Comparison of tested bar stress with predictions considering impact energy loss.

$$f_{sdmg} = \frac{1}{1.56D_{mg} - 0.25} \times f_{sd} \leq f_{yd} \quad (9d)$$

for Hwang et al. method

$$D_{mg} = \frac{E_l}{E_k} = \frac{m_{be}}{m_{be} + m_h} \quad (9e)$$

where f_{sd} =bar stress calculated from Eqs. (6) and (7); f_{yd} =dynamic yield strength; m_{be} =equivalent mass of the RC beam showing elastic deflection; and m_h =drop hammer mass.

Figure 13 compares the test results f_{test} with the bar stress predictions f_{sdmg} considering the effects of strain rate, cover concrete loss, and impact energy loss on the bond strength. The modified ACI 408-03 (ACI (American Concrete Institute) 2003) showed the best prediction with the average values = 1.09 and 0.81, and COV. = 0.16 and 0.12 for non-yielded and yielded bars, respectively. The prediction of the modified Hwang et al. (2017) method was comparable to that of ACI 408-03 (ACI (American Concrete Institute) 2003), showing the average values = 1.06 and 0.81, and COV. = 0.20 and 0.20 for non-yielded and yielded bars, respectively. It is noted that unlike the non-yielded bars, the average value smaller than 1.0 for yielded bars indicates the accurate and safe design result because of bond failure after reinforcing bar yielding.

6 Summary and conclusions

In the present study, lap splice tests were performed under impact load to investigate the effect of strain rate on the bond strength between reinforcing bars and concrete. Twenty-four RC beam specimens using D18 and D25 bars with the bar splice lengths of 300 mm and 400 mm were tested under seven different drop heights and three different hammer masses. A modification method was proposed to predict the tensile strength of bar splices under impact load, and it was compared with the test results. The primary results can be summarized as follows.

- 1) Bond failure occurred in test specimens under impact load, as the bar development length was smaller than the required development length under static load. Under low impact energy, the tensile strength of bar splices was greater than that of static load due to strain rate effect, but it was smaller than the dynamic yield strength. On the other hand, under large impact energy, the tensile strength of bar splices was greater than the dynamic yield strength, but bond failure occurred at once due to cover concrete damage.

- 2) The peak impact force, maximum mid-span deflection, residual mid-span deflection, maximum strain of reinforcing bars, and residual strain of reinforcing bars increased as the impact energy (i.e., impact velocity) increased. In the case of the same bar development length, the larger bar diameter showed the larger impact resistance, but the bond strength was identical regardless of the bar diameter. In the case of the same bar diameter, the longer development length showed the larger tensile strength of bar splices. In the case of the same impact energy, the heavier drop mass (i.e., the lower drop height) caused less energy loss, which increased the impact damage and bar strain in beam specimens.
- 3) The bond strength was increased by the strain rate effect on concrete at extremely short collision duration, and then decreased by cover concrete damage, which caused bond failure. The predicted bar stress based on the strain rate effect on concrete tensile strength was overestimated in the specimens without bar yielding, because in the existing design method for bar development length, earlier bond failure caused by cover concrete spalling along the bar development length was not considered.
- 4) The tensile strength of bar splices estimated from the existing design methods was conservative in the test specimens under large impact energy. When the dynamic concrete tensile strength and cover concrete loss were considered, the predicted bar stress under impact load showed the same tendency to that under static load. This is because the cover concrete loss sharply decreased the bond strength.
- 5) Modification factors for bar stress prediction in existing methods were proposed to address the effect of effective impact energy on the bond strength. The proposed method predicted well the test results.

According to the parameter ranges used in the present study, the proposed method is limited to D18 and D25 bars, splice length = 300 and 400 mm, concrete strength = 30–38 MPa, and impact energy = 8.22–33.66 kJ. However, because of bond failure in the majority of specimens, further researches are needed to evaluate the impact loading effect on the bond strength and bond-slip behavior in wide design parameters.

Acknowledgements

This research was financially supported by National Key Research Program of China (2016YFC0701400) and National Natural Science Foundation of China (Grant No. 51851110760 and 51878268). The authors are grateful to the authorities for their supports.

Authors' contribution

HH designed the research methodology; FY and LZ performed the test, HH and LZ draft the manuscript; JB and GM reviewed the manuscript; HH and

FY revised the final manuscript. All authors read and approved the final manuscript.

Authors' information

Hyeon-Jong Hwang, Assistant Professor, School of Architecture, Konkuk University, Seoul 05029, Republic of Korea.

Fan Yang, Graduate Student, Key Laboratory for Damage Diagnosis of Engineering Structures of Hunan Province, College of Civil Engineering, Hunan University, Changsha 410082, China.

Li Zang, Graduate Student, Key Laboratory for Damage Diagnosis of Engineering Structures of Hunan Province, College of Civil Engineering, Hunan University, Changsha 410082, China.

Jang-Woon Baek, Assistant Professor, Department of Civil Engineering and Environmental Sciences, Korea Military Academy, Seoul 01805, Republic of Korea.

Gao Ma, Associate Professor, Key Laboratory for Damage Diagnosis of Engineering Structures of Hunan Province, College of Civil Engineering, Hunan University, Changsha 410082, China.

Availability of data and materials

The data used to support the findings of this study are available from the authors upon request.

Competing interests

The authors declare that they have no competing interest.

Author details

¹ School of Architecture, Konkuk University, Seoul 05029, Republic of Korea.

² Key Laboratory for Damage Diagnosis of Engineering Structures of Hunan Province, College of Civil Engineering, Hunan University, Changsha 410082, China. ³ Department of Civil Engineering and Environmental Sciences, Korea Military Academy, Seoul 01805, Republic of Korea.

Received: 14 August 2019 Accepted: 5 May 2020

Published online: 21 August 2020

References

- ACI (American Concrete Institute). (2003). "Bond and development of straight reinforcing bars in tension (ACI 408R-03)." *ACI Committee 408*, Farmington Hills, MI, 1-48.
- ACI (American Concrete Institute). (2019). "Building code requirements for structural concrete and commentary." *ACI Committee 318*, Farmington Hills, MI, 1-623.
- ASTM. (2018). Standard test method for compressive strength of cylindrical concrete specimens. C39, West Conshohocken, PA.
- Biggs, J. M. (1964). *Introduction to Structural Dynamics*. New York: McGraw-Hill Book Company.
- Bischoff, P. H., & Perry, S. H. (1991). Compressive behaviour of concrete at high strain rates. *Materials and Structures*, 24(6), 425-450.
- Comite Euro-International du Beton. (1988). *Concrete Structures under Impact and Impulsive Loading* (p. 187). CEB Bulletin: Lausanne, Switzerland.
- Eurocode 2 (British Standards Institution). (2004). "Design of concrete structures. London, UK, 1-225.
- Fib. (2010). *fib Model Code for Concrete Structures* (pp. 1-420). Germany: Ernst & Sohn.
- Fujikake, K., Li, B. and Soeum, S. (2009). "Impact Response of Reinforced Concrete Beams and its Analytical Evaluation." *J. Struct. Eng.*, ASCE, 135(8), 938-950.
- Hansen, R. J., & Liepins, A. A. (1962). Behavior of bond under dynamic loading. *ACI J. Proc.*, 59(4), 563-583.
- Hughes, G., & Beeby, A. W. (1982). Investigation of the effects of impact loading on concrete beams. *Journal of the Structural Engineering. American Society of Civil Engineers*, 60B(3), 45-52.
- Hwang, H. J., Kang, T. H.-K., & Kim, C. S. (2019a). Numerical model for flexural behavior of rc members subjected to low-velocity impact loads. *ACI Struct. J.*, 116(2), 65-76.
- Hwang, H. J., Park, H. G., & Yi, W. J. (2017). Nonuniform bond stress distribution model for evaluation of bar development length. *ACI Struct. J.*, 113(1-6), 839-849.
- Hwang, H. J., Zang, L., & Ma, G. (2019b). Effect of impact loading on bar development length in CCT node. *Journal of Structural Integrity and Maintenance*, 4(1), 26-36.
- Ishikawa, N., Katsuki, S., and Takemoto, K. (2002). "Dynamic Analysis of Prestressed Concrete Beams under Impact and High Speed Loadings." *Proc. of 6th Int. Conf. on Structures under Shock and Impact*, WIT Press, Southampton, 247-256.
- Jacques, E., & Saatcioglu, M. (2019a). High strain rate bond characteristics of reinforced concrete beam-ends. *International Journal of Impact Engineering*, 130, 192-202.
- Jacques, E., & Saatcioglu, M. (2019b). Bond-slip modelling of reinforced concrete lap splices subjected to low and high strain rates. *Engineering Structures*, 195, 568-578.
- Jacques, E., & Saatcioglu, M. (2020). High strain rate response of reinforced concrete lap-spliced beams. *Journal of Structural Engineering, ASCE*, 146(1), 04019165.
- Kent, D. C., and Park, R. (1971). "Flexural Members with confined concrete." *Proc., ASCE*, 97(7), 1969-1990.
- Kishi, N., Ikeda, K., Mikami, H., and Yamaguchi, E. (2001). Dynamic behavior of rc beams under steel weight impact loading-effects of nose-shape of steel weight *Proc. of 3rd Int. Conf. on Concrete under Severe Conditions*, Univ. of British Columbia, Vancouver, Canada, 660-667.
- Kulkarni, S. M., & Shan, S. P. (1998). Response of reinforced concrete beams at high strain rates. *ACI Struct. J.*, 95(6), 705-715.
- Li, M., & Li, H. (2011). Effects of strain rate on reinforced concrete beam. *J. Adv. Mater. Research*, 243-249, 4033-4036.
- Li, B., Park, R., & Tanaka, H. (2000). Constitutive behavior of high-strength concrete under dynamic loads. *ACI Struct. J.*, 97(4), 619-629.
- Malvar, L. J., & Ross, C. A. (1998). Review of strain rate effects for concrete in tension. *ACI Materials Journal*, 95(6), 735-739.
- Mattock, A. H. (1967). Discussion of rotational capacity of reinforced concrete beams. *J. Struct. Div.*, 93(ST2), 519-522.
- Ou, Y. C., & Nguyen, N. D. (2014). Plastic hinge length of corroded reinforced concrete beams. *ACI Struct. J.*, 111(5), 1049-1058.
- Panteki, E., Máca, P., & Häußler-Combe, U. (2017). Finite element analysis of dynamic concrete-to-rebar bond experiments in the push-in configuration. *International Journal of Impact Engineering*, 106, 155-170.
- Paschen, H., Steinert, J., & Hjorth, O. (1974). *Untersuchungen über das Verbundverhalten von Betonstählen bei Kurzzeitbeanspruchung*. TU Braunschweig: Forschungsbericht.
- Rezansoff, T. M. P. Bufkin, J. O. Jirsa, and J. E. Breen. (1975). "The performance of lapped splices under rapid loading." Research Rep. No. 154-2. Austin, TX: Center for Highway Research, Univ. of Texas at Austin.
- Scott, B. D., Park, R., & Priestley, M. J. N. (1982). Stress-strain behavior of concrete confined by overlapping hoops at low and high strain rates. *ACI Struct. J.*, 79(1), 13-27.
- Shah, I. K., & Hansen, R. J. (1963). *Behavior of bond under dynamic loading*. Cambridge: Dept. of Civil Engineering, Massachusetts Institute of Technology.
- Solomos, G., & Berra, M. (2010). Rebar pullout testing under dynamic Hopkinson bar induced impulsive loading. *Materials and Structures*, 43(1-2), 247-260.
- Soroushian, P., & Choi, K. (1987). Steel mechanical properties at different strain rates. *Journal of the Structural Engineering. American Society of Civil Engineers*, 113(4), 663-672.
- Spacone, E., and El-Tawil, S. (2004). "Nonlinear Analysis of Steel-Concrete Composite Structures: State of the Art." *J. Struct. Eng.*, ASCE, 130(2), 159-168.
- Suzuki, S., Katsuki, S., Ishikawa, N., Ishikawa, Y., & Furukawa, K. (1996). A fundamental study on local dissipated energy and rheology model at impact point of concrete specimen by the pendulum impact test. *Journal of Structural Mechanics and Earthquake Engineering*, 36(543), 91-105. (in Japanese).

Toikka, L., Braimah, A., Razaqpur, G., & Foo, S. (2015). Strain rate effect on development length of steel reinforcement. *Journal of the Structural Engineering. American Society of Civil Engineers*, 141(11), 04015044.

Wakabayashi, M., Nakamura, T., Yoshida, N., Iwai, S. and Watanabe, Y. (1980). "Dynamic Loading Effects on the Structural Performance of Concrete and Steel materials and Beams." *Proc. 7th World Conf. on Earthquake Engineering*, Turkish National Committee on Earthquake Engineering, Istanbul, Turkey.

Yang, G., & Lok, T. (2007). Analysis of RC structures subjected to air-blast loading accounting for strain rate effect of steel reinforcement. *International Journal of Impact Engineering*, 34(12), 1924–1935.

Publisher's Note

Springer Nature remains neutral with regard to jurisdictional claims in published maps and institutional affiliations.

Submit your manuscript to a SpringerOpen[®] journal and benefit from:

- ▶ Convenient online submission
- ▶ Rigorous peer review
- ▶ Open access: articles freely available online
- ▶ High visibility within the field
- ▶ Retaining the copyright to your article

Submit your next manuscript at ▶ [springeropen.com](https://www.springeropen.com)
